Theoretical Modeling of Relativistic Iron Lines

Thomas Dauser
supervised by Jörn Wilms

Contents

1 Introduction to Black Hole Physics

1.1 Emitted Spectrum

The process of accretion is responsible for the energy release of galactic black holes (GBH) and active galactic nuclei (AGN). Due to the angular momentum of the matter which falls onto these

objects, an accretion disk is created. Simulations show that Magento-Hydrodynamic effects seem to transport angular momentum radially inwards. This heats the disk in return and in the case of GBHs the temperatures can be as high as $k_{\mathrm{B}}T \simeq 1\,\mathrm{keV}$ in the inner regions of the disk. The photons emitted by the disk are up-scattered by inverse comptonization in a corona of hot electrons. These hard X-ray photons are distributed according to a power law $E^{-\alpha}$. At photon energies around the temperature of the corona this power law behavior breaks down exponentially, as the hot gas cannot supply the photons with more energy.

1.2 Fluorescent Emission in Strong Gravity Regime

Some of these hard X-rays can now irradiate the relatively cold accretion disk. Depending on the ionization of the disk, this leads to a spectrum of several emission lines. Figure 1 shows the result of a Monte Carlo simulation of a spectrum from a neutral disk which is irradiated by photons, distributed according to a power law. Higher ionized disks show less emission features
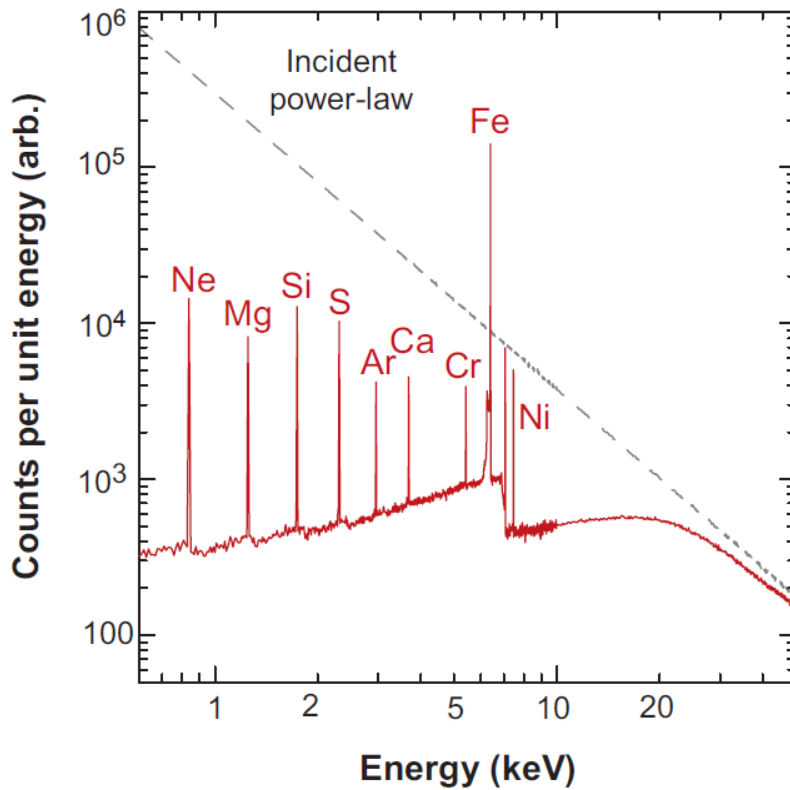
Figure 1: A Monte Carlo simulation of a spectrum from neutral disk which is irradiated by photons distributed according to a power law (taken from Miller (2007), who adapted it from Reynolds (1996))

and stronger absorption edges up to no signatures at all for fully ionized disks.

Due to abundances and fluorescent yield the Fe Kα with an energy of 6.4 keV is usually the

strongest and therefore often the only emission feature present in the X-ray spectrum.

1.3 Measuring the Spin of a Black Hole

In the vicinity of a black hole there a several features which modify the narrow emission line to a broad and mostly double peaked feature, where the spacetime around the black hole is imprinted. As the spacetime depends on the spin of the black hole a, it is possible to measure it by fitting a sophisticated modeled line to the data. Figure 2 shows observations of MCG-6-30-15, which are
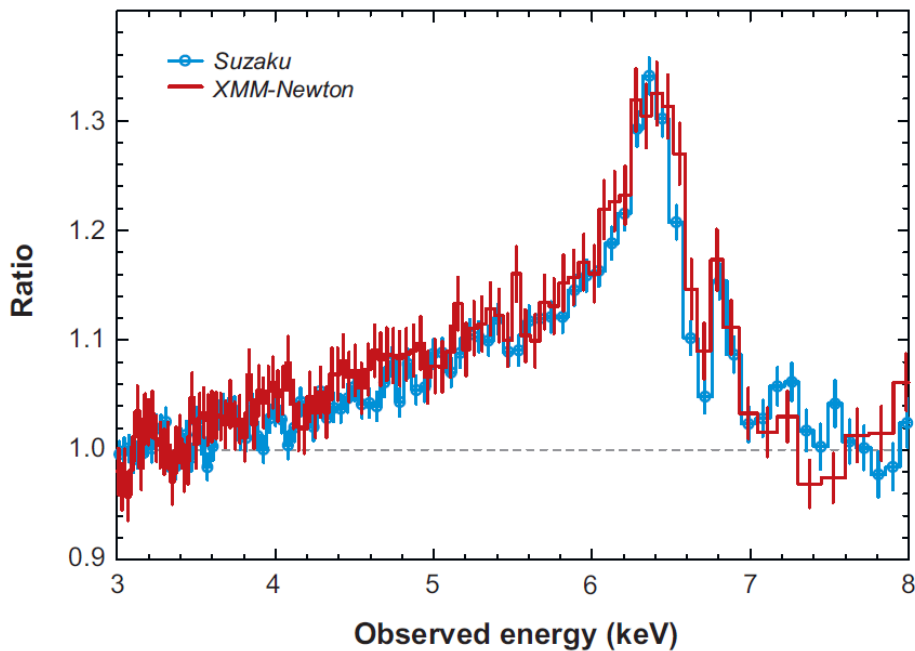
Figure 2: Observations of MCG$-6-30-15$, which is the best observation of a relativistic iron line in an AGN. Taken from Miller (2007), adapted from Miniutti et al. (2007) and Reeves et al. (2006).

the best spectra of relativistic iron lines in active galactic nuclei (AGN) up to now.

Nevertheless Dovčiak et al. (2004) come to the conclusion that it is not possible to measure the spin of MCG-6-30-15 with this method. Their statement is based on the `kyrline` model. Two years later, Brenneman & Reynolds (2006) claim that they determined the spin in the long XMM-Newton observation with their `kerrdisk` model to $0.989^{+0.009}_{-0.002}$. In contrast to Dovčiak et al. they take additional constraints into account by neglecting emission from within the innermost stable circular orbit (ISCO). According to most theoretical considerations this seems to be justified. Additionally they explicitly rule out a Schwarzschild black hole, as for $a = 0$ no reasonable model was found to describe the data, despite even including emission from within the ISCO. This makes the analysis especially robust and clearly shows that it is possible to measure the spin of a black hole by modelling the shape of the iron line.

This discrepancy between the results points towards the issue that the models might predict

different shapes of the relativistic emission line, which might affect the analysis. As the models are very differently sized because of their precalculated tables and use different interpolation techniques, some kind of difference could easily arise.

The *aim of this work* is to compare the existing models in order to see if they predict differences in the line shapes and whether this has concequences for for the data analysis.

2 Basic Theory on Spinning Black Holes

After having convinced ourselves, that emission lines are present in the spectrum and that this might be useful for determining the spin of black holes, the next step is to derive a theoretical model of their shape. This would provide us with the required connection between observed line and spin. As spacetime around black holes is highly relativistic, it absolutely necessary to perform all calculations in a fully relativistic way.

In the following all formulas are given in units such that the gravitational constant and the velocity of light are equal to one ($G = c = 1$).

2.1 The Metric

In General Relativity (GR), a spinning black hole can be described by the Kerr metric (Kerr, 1963), as this solves the Einstein equation for a spinning, spherical mass. It is fully determined by the mass M and the angular momentum J, which will be parameterized by $a = J/M$. Then line element reads

$$\mathrm{d}s^2 = -\left(1 - \frac{2Mr}{\Sigma}\right)\mathrm{d}t^2 - \frac{4aMr\sin^2\theta}{\Sigma}\mathrm{d}t\mathrm{d}\varphi \tag{1}$$

$$+ \frac{\Sigma}{\Delta}\mathrm{d}r^2 + \Sigma\mathrm{d}\theta^2 + \left(r^2 + a^2\frac{2a^2Mr\sin^2\theta}{\Sigma}\right)\sin^2\theta\mathrm{d}\varphi^2 \quad,$$

where $\Delta = r^2 - 2Mr + a^2$ and $\Sigma = r^2 + a^2\cos^2\theta$. This is the Boyer-Lindquist coordinate system. Here the black hole is spinning in φ-direction. In the case of a non-rotating black hole, this solution can easily be reduced to the Schwarzschild metric by setting $a = 0$:

$$\mathrm{d}s^2 = -\left(1 - \frac{2Mr}{\Sigma}\right)\mathrm{d}t^2 + \left(1 - \frac{2Mr}{\Sigma}\right)^{-1}\mathrm{d}r^2 + r^2\mathrm{d}\theta^2 + r^2\sin^2\theta\mathrm{d}\varphi^2 \tag{2}$$

As the Kerr metric is axi-symmetric and stationary, there exist two Killing vectors which characterize the conserved quantities. As expected from classical mechanics, where the conserved energy originates from invariance under time translation, the time-like Killing vector $K^\mu = (\partial_t)^\mu$ in GR can be used to define the total energy of stationary system E_R (the Komar energy). It can be shown straight forward (Carroll, 2004), that this is equal to the mass $E_R = M$ given in Eq. 1. In analogy, the conserved angular momentum J_R can be defined using the rotational Killing vector $R^\mu = (\partial_\varphi)^\mu$ due to the axis-symmetry. This leads to $J_R = aM = J$ and confirms the above interpretation of J as angular momentum.

As the disk is thought to be stable, it seems reasonable that angular momentum might build up towards the maximum value of $a = 1$. But in fact it is never possible to reach this value, as negative angular momentum orbits are more likely for higher a. Thorne (1974) used the exact angular distribution of thermal photons originating from an accretion disk and showed that the limit is $a \simeq 0.998$.

2.2 Spacetime in the Kerr Metric

A stationary observer, which sits at a point (r, θ) should not feel any changes of the metric by definition. This implies for our choice of coordinates implies that he has to rotate with angular velocity

$$\Omega = \frac{\mathrm{d}\varphi}{\mathrm{d}t} = \frac{u^\varphi}{u^t} \tag{3}$$

with respect to an observer which rests at infinity. Here the definition of the four-velocity is $u^\mu = \mathrm{d}x^\mu/\mathrm{d}\tau$, where τ is the proper time of a comoving observer. The total four velocity of this observers then becomes

$$\vec{u} = u^t \partial_t + u^\varphi \partial_\varphi = u^t \left(\partial_t + \Omega \partial_\varphi \right) \quad . \tag{4}$$

Using that $\vec{u}^2 = -1$ leads to

$$\begin{aligned}
-1 &\overset{!}{=} u^\mu u_\mu \\
&= (u^t)^2 \left[(\partial_t)^\mu (\partial_t)_\mu + 2(\partial_\varphi)^\mu (\partial_t)_\mu + (\partial_\varphi)^\mu (\partial_\varphi)_\mu \right] \\
&= (u^t)^2 \left(g_{tt} + 2\Omega g_{t\varphi} + g_{\varphi\varphi} \right)
\end{aligned} \tag{5}$$

which means that we derived an expression for the velocity in t-direction:

$$u^t = \frac{1}{\sqrt{-g_{tt} - 2\Omega g_{t\varphi} - g_{\varphi\varphi}}} \tag{6}$$

This equation shows nicely that $u^t > 0$, which means that $\vec{u}$ lies in the future light cone. Moreover, the expression under the root hast to be positive. This sets an additional condition on the angular velocity:

$$\Omega_{\min} = \frac{1}{g_{\varphi\varphi}} \left[-g_{t\varphi} - \sqrt{g_{t\varphi} - g_{tt} g_{\varphi\varphi}} \right] < \Omega < \frac{1}{g_{\varphi\varphi}} \left[-g_{t\varphi} - \sqrt{g_{t\varphi} + g_{tt} g_{\varphi\varphi}} \right] = \Omega_{\max} \tag{7}$$

For a non spinning black hole, this just restricts particles to move slower than c. Taking a closer look at $\Omega_{\min}$ reveals, that it becomes zero at a radius

$$r_0 = M + \sqrt{M^2 - a^2 \cos^2 \theta} \quad , \tag{8}$$

called the *static limit*. This means that static observers ($\Omega = 0$) are forbidden, which are closer than this radius to the black.

Moving nearer to the black hole, the event horizon is finally reached where there is only one possible value, with $\Omega_{\min} = \Omega_{\max}$. Following Carroll (2004), the event horizon at a radius r_H is uniquely characterized by the condition $g^{rr}(r_H) = 0$. In the case of the kerr metric this means $\Delta \overset{!}{=} 0$, which results in a radius of

$$r_\pm = M \pm \sqrt{M^2 - a^2} \quad . \tag{9}$$

The region between the *event horizon* and the static limit is called the *ergosphere*. As explained above, an observer in this region has no choice but to rotate in the direction of the black hole. This phenomena is called *dragging of inertial frames* and leads to strange consequences such that it is ideed possible to dive into this zone and extract energy from the black hole. For further details on that see Carroll (2004).

2.3 Equations of Motion

Determining the motion of particles and photons means calculating the evolution of $x^\mu(\lambda)$. This is described by the *Geodesic Equation*:

$$\frac{\mathrm{d}^2 x^\mu}{\mathrm{d}\lambda^2} + \Lambda^\mu_{\rho\sigma} \frac{\mathrm{d}x^\rho}{\mathrm{d}\lambda} \frac{\mathrm{d}x^\sigma}{\mathrm{d}\lambda} = 0 \tag{10}$$

Equivalent to classical mechanics, it is possible achieve the same relations more elegantly by using the Lagrangian or Hamiltonian formalism. As Krolik (1999) shows, the relativistic generalization can be done by redefining the action

$$S = \int_{A^\mu}^{B^\mu} \mathcal{L} \, \mathrm{d}\lambda = \int_{A^\mu}^{B^\mu} \mathrm{d}\lambda \left[g_{\mu\nu} \frac{\mathrm{d}x^\mu}{\mathrm{d}\lambda} \frac{\mathrm{d}x^\nu}{\mathrm{d}\lambda} \right]^{-\frac{1}{2}} \quad . \tag{11}$$

Minimizing it along the path by means of variation leads to the geodesic equation, which confirms that th Lagrangian describes the same movement. For massive particles one can set $\lambda = \tau$ and easily sees that the Lagrangian is constant along the path, which is a crucial requirement. This can not be done for a photon, as its proper time is zero. Following Krolik (1999), choosing $\tau = \lambda\mu$ and an effective Lagrangian

$$\mathcal{L}_{\text{eff}} = \frac{1}{2} g_{\mu\nu} \dot{x}^\mu \dot{x}^\nu \quad , \tag{12}$$

solves this problem and leads to the same dynamical equations. As λ is an arbitrary parameter, we now can describe photons by $\mu = 0$ and massive particles by $\mu = 1$.

As we reduced our problem to a known formalism, calculating the Hamiltonian $H = p_\mu \dot{x}^\mu - \mathcal{L}_{\text{eff}}$ and the momentum $p_\mu = \frac{\partial \mathcal{L}}{\partial x^\mu} = g_{\mu\nu} \dot{x}^\nu$ is now straight forward:

$$\begin{aligned}
H =& \frac{1}{2\Sigma} \left(\Delta p_r^2 + p_\theta^2 - \frac{(r^2 + a^2)^2 - a^2 \Delta \sin^2\theta}{\Delta} p_t^2 + \frac{\Delta - a^2 \sin^2\theta}{\Delta \sin^2\theta} p_\varphi^2 - \frac{4Mar}{\Delta} p_t P_\varphi \right) \\
p_t =& - \left(1 - \frac{2Mr}{\Sigma} \right) \dot{t} - 2Mar \frac{\sin^2\theta}{\Sigma} \dot{\varphi} \\
p_r =& \frac{\Sigma}{\Delta} \dot{r} \\
p_\theta =& \Sigma \dot{\theta} \\
p_\varphi =& \left(r^2 + a^2 + 2Ma^2 r \frac{\sin^2\theta}{\Sigma} \right) \sin^2\theta \dot{\varphi} - 2Mar \frac{\sin^2\theta}{\Sigma} \dot{t}
\end{aligned} \tag{13}$$

The derivations of the Hamiltonian $\partial_\mu H = -\dot{p}_\mu$ with respect to t and φ are zero, which immediately lead to the conserved energy $p_t = -E$ and angular momentum $p_\varphi = L$. Additionally the constancy of the Hamiltonian describes the conservation of the test particles rest mass $H = -1/2\mu^2$. A last conserved quantity $\mathcal{Q} = p_\theta^2 + \cos^2\theta[a^2(\mu^2 - p_t^2) + p_\varphi^2/\sin^2\theta]$ was found by Carter (1968), which can be shown be making a separation ansatz in the Hamilton-Jacobi formalism with respect to θ and r. Now the equations of motion are fully determined and length

algebraic calculations (see Bardeen et al. (1972)) lead to

$$\Sigma \dot{t} = -a(aE\sin^2\theta - L) + (r^2 + a^2)\frac{T}{\Delta}$$
$$\Sigma \dot{r} = \pm\sqrt{V_r}$$
$$\Sigma \dot{\theta} = \pm\sqrt{V_\theta}$$
$$\Sigma \dot{\varphi} = -\left(aE - \frac{L}{\sin^2\theta}\right) + a\frac{T}{\Delta} \quad , \tag{14}$$

for which we defined

$$T = E(r^2 + a^2) - aL$$
$$V_r = T^2 - \Delta\left(\mu^2 + r^2 + (L - aE)^2 + \mathcal{Q}\right)$$
$$V_\theta = \mathcal{Q} - \cos^2\theta\left(\frac{L^2}{\sin^2\theta} + a^2(\mu^2 - E^2)\right) \quad . \tag{15}$$

The upper sign in front of $\pm\sqrt{V_r}$ describes the movement towards the black hole in r-direction and respectivly the lower sign has to be taken for the orbits away from it. For the θ-direction this definition is similar.

2.3.1 The Accretion Disk

Having developed the general equations of motion in the Kerr metric, we now want to apply them to describe a thin accretion disk, which lies in the equator plane of the black hole. This implies that

$$\theta = \pi/2 \quad \text{and} \quad \dot{\theta} = 0 \tag{16}$$

and therefore $\mathcal{Q} = 0$. The accretion disk itself is most easily modeled by particles which move on infinitely many circular orbits of different radii. This means that the velocity and the acceleration in r-direction has to vanish:

$$\dot{r} = 0 \quad \overset{\text{Eq. 14}}{\longrightarrow} \quad V_r(r) = 0 \quad \text{and} \quad \ddot{r} = 0 \quad \overset{\text{Eq. 14}}{\longrightarrow} \quad \frac{\mathrm{d}V_r(r)}{\mathrm{d}r} = 0 \tag{17}$$

Additionally we want the accretion disk to be stationary, because the equations we calculated before are only valid in this case. These informations are enough to fully determine the trajectories of the particles, which has been done in detail by Bardeen et al. (1972). The results will be motivated in the following.

They first calculated the explicit expressions of E and L. Using this, the angular velocity of the stationary accretion disk becomes

$$\Omega = \frac{\mathrm{d}\varphi}{\mathrm{d}t} = \pm\frac{\sqrt{M}}{r\sqrt{r} \pm a\sqrt{M}} \quad , \tag{18}$$

where the upper sign refers to corotating particles and the lower to retrograde orbits. Assuming stable orbits of the particles in order to form an accretion disk imposes additionally that
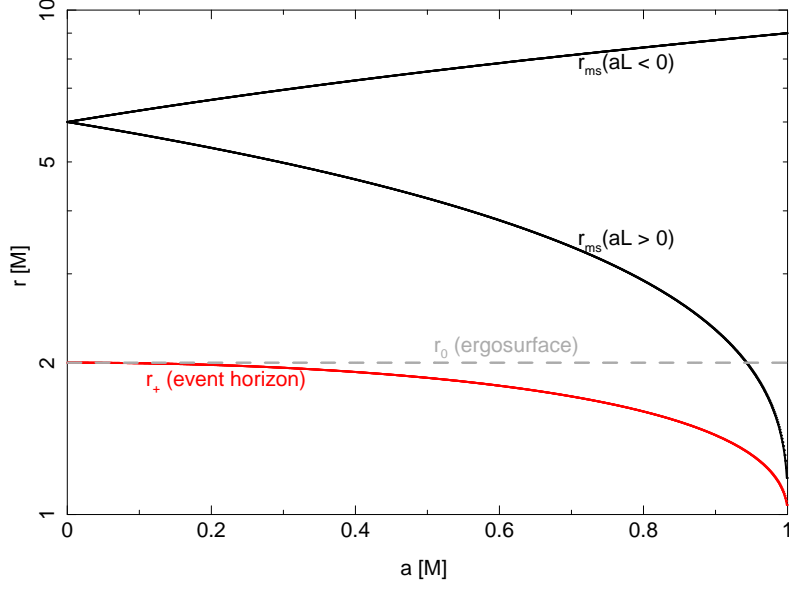
Figure 3: This plot shows the evolution of all important surfaces around Kerr Black Holes with respect to their angular momentum a. It is plotted for $\theta = \pi/2$, as this is the plane of the accretion disk.

$$\frac{\mathrm{d}^2 V_r(r)}{\mathrm{d}r^2} \leq 0 \quad , \tag{19}$$

which is sufficient for stability as $V_r(r) \geq 0$. Solving this system of equations reveals that only radii $r \geq r_{\mathrm{ms}}$ are stable, with

$$r_{\mathrm{ms}} = M \left(3 + Z_2 \mp \sqrt{(3 - Z_1)(3 + Z_1 + 2Z_2)} \right) \tag{20}$$

$$Z_1 = 1 + (1 - a^2)^{1/3} \left[(1 + a)^{1/3} + (1 - a)^{1/3} \right]$$

$$Z_2 = \sqrt{3a^2 + Z_1^2} \quad . \tag{21}$$

This means that the accretion disk only extends down to a certain radius of *marginal stability*, which for example gives

$$r_{\mathrm{ms}} = \begin{cases} 1.237\,M & \text{for } a = 0.998 \\ 6\,M & \text{for } a = 0 \\ 8.994\,M & \text{for } a = -0.998 \end{cases} \tag{22}$$

Fig. 3 shows a summary of the evolution of all important radii mentioned above with respect to a. Using Eq. 4, the four-velocity of the particles building the accretion disk can be derived as

$$\vec{u} = u^t \left(\partial_t + \Omega \partial_\varphi \right), \ \text{with } u^t = \frac{r\sqrt{r} \pm a\sqrt{M}}{\sqrt{r}\sqrt{r^2 - 3Mr \pm 2a\sqrt{M}\sqrt{r}}} \quad . \tag{23}$$

Clearly it is also possible to extract the trajectories for $r \leq r_{\mathrm{ms}}$ from the equations above. As the orbits are not stable, the particles fall towards the event horizon with the energy $E(r_{\mathrm{ms}})$ and angular momentum $L(r_{\mathrm{ms}})$ they have at the radius of marginal stability. This implies that the particles might have a non-zero velocity and acceleration in r-direction and therefore their total four-velocity is given by $\vec{u} = u^t \partial_t + u^r \partial_e + u^{\varphi} \partial_{\varphi}$. As we will not need this trajectories in the following and the equations are rather lengthy they are not written here. Interested readers can find them at Speith et al. (1995).

2.3.2 Photon Trajectories

Having described the location and frame where the photons are emitted, we now want to follow their way to the observer. Due to the large distance to the black hole system, we will only see photons which fly exactly in our direction. This means by looking at the system under different angles we will clearly measure different photons and obtain different results for the line shape. Thus it is only important to consider photons, which travel at infinity in the same direction. This chapter follows the detailed descriptions of Chandrasekhar (1983).

The photons originate from the stationary and axi-symmetric accretion disk, which implies that we only have to consider the (r, θ) plane simply because of the symmetrical reasons. This leaves us with only two equations of motion from Eq. 14. Integrating over the path from the point of emission at the accretion disk $(r_{\mathrm{e}}, \pi/2)$ to the observer at infinity (∞, θ_0) leads to

$$\int_{r_{\mathrm{e}}}^{\infty} \frac{\mathrm{d}r}{\sqrt{V_r}} = \int_{\pi/2}^{\theta_0} \frac{\mathrm{d}\theta}{\sqrt{V_{\theta}}} \quad . \tag{24}$$

Additionally one has to take into account, that the photons might have turning points in r and θ-direction. This means that the integration has to be split into different parts. The final solution will be a combination of them, which accounts for the different paths the photon can take to reach the distant observer.

Examining the possible parameter space of Eq. 24 quickly leads to the conclusion that the roots require

$$V_r(r) \geq 0 \qquad \text{and} \qquad V_{\theta}(\theta) \geq 0 \tag{25}$$

for a real solution. The limits determined by there conditions can be identified with the turning points r_{t} and η_{t} (see Chandrasekhar (1983) for details). Taking into account that the sign changes at the turning point, the trajectories of the photons can be given. Without any turning points the integration of 24 can now be performed

$$\int_{r_{\mathrm{e}}}^{\infty} \frac{\mathrm{d}r}{\sqrt{V_r}} = -\int_{0}^{\eta_0} \frac{\mathrm{d}\eta}{\sqrt{V_{\eta}}} \quad , \tag{26}$$

where we defined $V_{\eta} := \sin^2 \theta V_{\theta}$ and substituted $\eta = \cos \theta$. Considering a turning point in θ-direction splits the integration over η in two parts:

$$\int_{r_{\mathrm{e}}}^{\infty} \frac{\mathrm{d}r}{\sqrt{V_r}} = -\int_{0}^{\sqrt{\eta_{\mathrm{t}}^2}} \frac{\mathrm{d}\eta}{\sqrt{V_{\eta}}} + \int_{\sqrt{\eta_{\mathrm{t}}^2}}^{\eta_0} \frac{\mathrm{d}\eta}{\sqrt{V_{\eta}}} \quad . \tag{27}$$

Looking at the case of the r-integration in a rough geometrical picture reveals, that the turning point can only occur if the black hole is between the point of emission and the observer. Otherwise the turning point of the photon would be closer to the black hole than the location where it was emitted, which can be considered as highly unlikely. Moreover a photon emitted behind the black hole requires in this picture a turning point in θ-direction in order to be seen by the observer. Thus we only need one last equation with a turning point for each direction:

$$-\int\limits_{r_\mathrm{e}}^{r_\mathrm{t}} \frac{\mathrm{d}r}{\sqrt{V_r}} + \int\limits_{r_\mathrm{t}}^{\infty} \frac{\mathrm{d}r}{\sqrt{V_r}} = -\int\limits_{0}^{\sqrt{\eta_\mathrm{t}^2}} \frac{\mathrm{d}\eta}{\sqrt{V_\eta}} + \int\limits_{\sqrt{\eta_\mathrm{t}^2}}^{\eta_0} \frac{\mathrm{d}\eta}{\sqrt{V_\eta}} \tag{28}$$

Solving these equations for a specific E and L now fully determines the movement of the photon. For means of easier calculation it is convenient to choose new integrals of motion

$$\lambda = \frac{L}{E} \qquad \text{and} \qquad q^2 = \frac{\mathcal{Q}}{E^2} \quad, \tag{29}$$

and multiply the $V_{r,\eta}$ with E^{-2}. This leads to

$$\begin{aligned} V_r &= r^4 + (a^2 - \lambda^2 - q^2)r^2 + 2M\left((a-\lambda)^2 + q^2\right)r - a^2 q^2 \\ V_\eta &= -a^2\eta^4 + (a^2 - \lambda^2 - q^2)\eta^2 + q^2 \quad. \end{aligned} \tag{30}$$

The momentum of the photon expressed in the most easiest way then reads

$$\begin{aligned} p_t &= -E \\ p_r &= \pm\frac{E}{\Delta\sqrt{V_r}} \\ p_\theta &= \pm E\sqrt{V_\theta} \\ p_\varphi &= E\lambda \quad. \end{aligned} \tag{31}$$

2.4 Transfer Function

So far, we described single photons that are emitted at the disk and selected the ones which we see under a view angle θ_0. In this section we will consider emission from the whole accretion disk, based on the model of a thin disk described in section 2.3.1. In its rest frame, the specific intensity at a certain energy I_{E_e} emitted at the surface depends only on the radius r_e and the emission angle n_e.

2.4.1 Radiation Transport

For an observer far away, the black hole is a point source. This means he can only see the whole disk at once and thus measures an integrated specific luminosity

$$L_{E_\mathrm{o}} = 4\pi d^2 \int I_{E_\mathrm{o}}(r_\mathrm{e}, n_\mathrm{e})\mathrm{d}\Omega \quad, \tag{32}$$

10
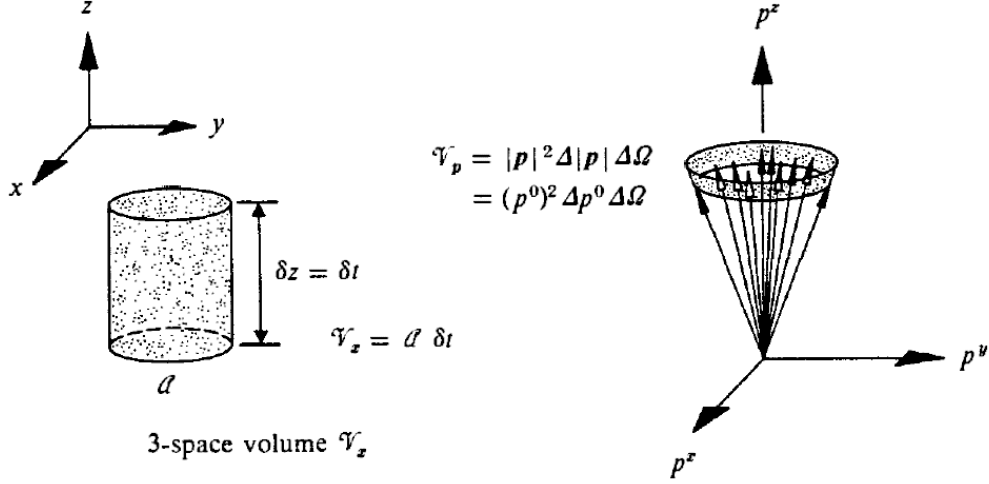
Figure 4: A drawing of volumes of the phase space $V_x V_P$, for the momentum space V_p and the normal space V_x, necessary to calculate the number density of trajectories $\mathcal{N}$ in curved space. (adapted from Misner et al., 1973)

where d is the distance to the system. The specific intensity of photons with energies between E and $E + \mathrm{d}E$ is defined by

$$I_E = \frac{E\mathrm{d}N}{\mathrm{d}A\mathrm{d}E\mathrm{d}\Omega\mathrm{d}t} \quad , \tag{33}$$

where $\mathrm{d}N$ is the number of photons in the solid angle $\mathrm{d}\Omega$ with energy E, which flow through the area $\mathrm{d}A$ in the time $\mathrm{d}t$. As these variables are clearly not Lorentz invariant, I_E is not a good quantity and will vary depending on the chosen frame of reference. Nevertheless we need to find a way to convert the emitted intensity I_{E_e} at the accretion disk to the measured intensity I_{E_o}, as they will not be equal in general. Following Misner et al. (1973), it can be shown that the number density $\mathcal{N} = \delta N / (V_x V_p)$ is an invariant, as

$$\mathrm{d}\mathcal{N}/\mathrm{d}\lambda = 0 \quad . \tag{34}$$

Here $V_x V_p$ is the phase space volume of N identical particles. Eq. 34 is the collisionless Boltzman equation in curved space, which can be easily derived from the general *Liouville theorem*. Explicit considerations (see Fig. 4) lead to $V_x = A\mathrm{d}t$ and $V_p = \mathrm{d}\Omega E^2 \mathrm{d}E$. As we required all particles to be the same, the relation $\vec{p}^2 = m^2$ stays constant and dictates the four momenta to lie on a hyperboloid. Now we can identify the specific intensity with the conserved number density and we get

$$\frac{I_E}{E^3} = \mathcal{N} = \mathrm{const.} \tag{35}$$

Now we finally obtained a connection between the observed and the locally emitted luminosity, reading

$$L_{E_\mathrm{o}} = 4\pi d^2 \int \left(\frac{E_\mathrm{o}}{E_\mathrm{e}}\right)^3 I_{E_\mathrm{e}}(r_\mathrm{e}, n_\mathrm{e})\mathrm{d}\Omega \quad . \tag{36}$$

11

The ratio $E_\mathrm{o}/E_\mathrm{e}$ between the observed and the emitted energy is exactly the definition of the redshift. Taking into account that the observer measures in a flat Minkowski space and using the expressions for the four-momentum of the photon, the redshift becomes

$$g = \frac{E_\mathrm{o}}{E_\mathrm{e}} = -\frac{E}{p_\mathrm{e}^\mu u_\mu} = \frac{\sqrt{r_\mathrm{e}}\sqrt{r_\mathrm{e}^2 - 3Mr_\mathrm{e} + 2a\sqrt{Mr_\mathrm{e}}}}{r_\mathrm{e}\sqrt{r_\mathrm{e}} + a\sqrt{M} - \sqrt{M}\lambda} \quad . \tag{37}$$

Keep in mind that E, the energy of the photon at infinity, is the very same as the conserved quantity, which describes the geodesic of the photon. Moreover this means if we know at which energy the photon is emitted from the disk and know its redshift, we can calculate the energy at which we should observe it. For easier calculation, we create an homogenius parameter space by redefining the redshift. Using the maximal and minimal redshift we define for each gas ring and incination angle the parameter

$$g^* := \frac{g - g_\mathrm{min}}{g_\mathrm{max} - g_\mathrm{min}} \quad , \qquad 0 \leq g^* \leq 1 \quad . \tag{38}$$

There can be up to two solutions for a specific g^* and a certain radius due to symmetric reasons. This can be easily visualized, as you clearly have two possibilities on a circle to get from the minimum to the maximum value of the redshift. As the redshift is a steady function, each value in between the extreme values appears twice.

The only unknown quantity left is the emission angle n_e. Due to the effects of strong gravity in the vicinity of the black hole, the photons do not travel on a straight path and are likely to be observed under a different angle. But the emission angle is already totally defined by the four-momentum of the emitted photon. With the normal vector to the disk $\vec{n}$ and the energy of the photon $-p_\mathrm{e}^\mu u_\mu$, these quantities are related by

$$\cos(n_\mathrm{e}) = \frac{\vec{p}_{\mathrm{e}\perp}}{|\vec{p}_\mathrm{e}|} = -\frac{p_\mathrm{e}^\mu n_\mu}{p_\mathrm{e}^\mu u_\mu} = -\frac{p_\mathrm{e}^\mu n_\mu}{E}g \quad , \tag{39}$$

where we used Eq. 37 for the last equality. Furthermore the normal vector can be expressed by

$$\vec{n} = \left. \frac{1}{\Sigma}\partial_\theta \right|_{\theta=\pi/2} \quad , \tag{40}$$

as it is defined as a spatial vector perpendicular to the accretion disk. Using the the four mometum of the photon from Eq. 31, the fact that $\eta^2|_{\pi/2} = 0$ and the expression for V_η (Eq. 30), the angle becomes

$$\cos(n_\mathrm{e}) = \frac{qg}{r_\mathrm{e}} \quad . \tag{41}$$

2.4.2 Transfer Function of Cunningham

For means of calculation, Cunningham (1975) defined the *Transferfunction f*

$$f(g^*, r_\mathrm{e}, \theta_0) = \frac{d^2}{\pi r_\mathrm{e}} g\sqrt{g^*(1-g)} \left| \frac{\partial\Omega}{\partial(g^*, r_\mathrm{e})} \right| \quad . \tag{42}$$

Using the relations calculated in this section, the total observed luminosity becomes

$$L_{E_o} = \int\limits_{r_+}^{\infty} \int\limits_{0}^{1} 4\pi^2 r_e \frac{g^2}{g^*(1-g^*)} f(g^*, r_e, \theta_0) I_{E_e}(r_e, n_e) \mathrm{d}r_e \mathrm{d}g^* \tag{43}$$

Here we parametrized the accretion disk in (r_e, g^*) space. Because this leads to the conserved quantities λ and q the motion is still defined properly. Additionally we see, that a model describing the specific intensity is required. As we want to compare this to existent models, we make the same assumptions being

$$I_{E_e} \propto r_e^{-\alpha} \cdot f(n_e) \quad . \tag{44}$$

Thus the radial dependence is described by a power law characterized by the emissivity α. Usually values of $\alpha = 2$ - 3.5 are observed. Furthermore the intensity might depend on the emission angle. Here we chose the limb darkening model

$$f(n_e) = 1 + 2.06 \cos n_e \tag{45}$$

invented by Laor (1991), as the `laor` and the `kerrdisk` model use it. In contrast to that, recent theoretical considerations by Svoboda et al. (2009) show that limb brightening is more likely to occure. Moreover they explain that this would lower the emissivity index systematically, which is usually observed to be too high by using the limb darkening models.

2.4.3 Numerical Calculation

For the numerical evaluation of the transfer function we use a FORTRAN 77 code, developed by Speith et al. (1995). Therein the emission from the accretion disk is modeled by a grid in the (r_e, g^*)-space. As explained above, this is sufficient to describe the motion of the photons.

In order to evaluate the derivation of the solid angle and get rid of the d^2 dependence in Eq. 42 we use the impact parameters α and β, which were first defined by Cunningham & Bardeen (1973). They describe the how a distant observer sees the black hole, by projection of the photons on a plane perpendicular to the line of sight. This is drawn in Fig. 5. Now we express the impact parameters by the four momentum using simple geometric considerations as

$$\alpha = -d\frac{p^{(\varphi)}}{|p^{(\mu)}|} = -d\frac{p_\mu \left[e^{(\varphi)}\right]^\mu}{p_\mu \left[e^{(t)}\right]^\mu} \qquad \text{and} \qquad \beta = d\frac{p^{(\theta)}}{|p^{(\mu)}|} = d\frac{p_\mu \left[e^{(\theta)}\right]^\mu}{p_\mu \left[e^{(t)}\right]^\mu} \quad . \tag{46}$$

The coordinates written in brackets, to show that they are the coordinates of the observer living in a flat Minkowski space. Following Misner et al. (1973), the he aligns his tetrads according to

$$\vec{e}_{(t)} = \vec{u} \quad , \qquad \vec{e}_{(i)} = \vec{e}_{(i)}^{\,\mu} \partial_\mu \quad \text{and} \qquad \vec{e}_{(i)}^{\,\mu} \vec{e}_{(i)}^{\,\nu} g_{\mu\nu} = \eta_{(i)(j)} \quad , \tag{47}$$

where $\eta_{\mu\nu}$ is the Minkowski metric. Applying these conditions, the tetrads of an observer at rest
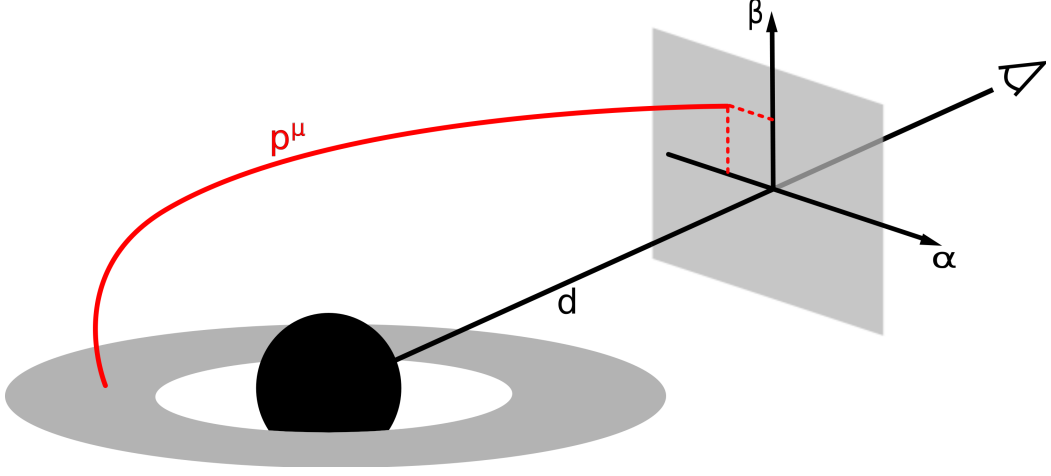
Figure 5: A drawing to clarify the definition of the impact parameters α and β. They describe how a distant observer would see the photons emitted around the black hole, which are projected perpendicular to his line of sight.

can be constructed. In spherical coordinates they read:

$$\vec{e}_{(t)} = \sqrt{\frac{\Sigma}{\Sigma - 2Mr}} \partial_t$$

$$\vec{e}_{(r)} = \sqrt{\frac{\Delta}{\Sigma}} \partial_r$$

$$\vec{e}_{(\theta)} = \frac{1}{\sqrt{\Sigma}} \partial_\theta$$

$$\vec{e}_{(\varphi)} = -\frac{2Mra}{\sqrt{\Sigma\Delta}} \sqrt{\frac{\sin^2\theta}{\Sigma - 2Mr}} \partial_r + \sqrt{\frac{\Sigma - 2Mr}{\Sigma\Delta\sin^2\theta}} \partial_\varphi \tag{48}$$

Combining the coordinate system of the observer with the four momentum of the emitted photon (Eq. 31), we can now derive the impact parameters with Eq. 46. As the observer is far away, we let d go to infinity and thus obtain

$$\alpha = -\frac{\lambda}{\sin\theta_0} \qquad \text{and} \qquad \beta = \pm\sqrt{V_\theta} \quad . \tag{49}$$

Furthermore the impact parameters are defined such that

$$d^2 \cdot \mathrm{d}\Omega = \mathrm{d}\alpha\mathrm{d}\beta = \left|\frac{\partial(\alpha,\beta)}{\partial(\lambda,q)}\right| \mathrm{d}\lambda\mathrm{d}q = \frac{q}{\sin\theta_0\beta}\mathrm{d}\lambda\mathrm{d}q \quad . \tag{50}$$

In this way we get rid of the apparent d^2 dependence and are able to calculate the partial derivative of the solid angle, which appears in the *Transferfunction* (Eq. 42). This leads to

$$d^2 \left|\frac{\partial\Omega}{\partial(g^*,r_\mathrm{e})}\right| = \frac{q(g_\mathrm{max} - g_\mathrm{min})}{\sin\theta_0\beta \left|\frac{\partial(g^*,r_\mathrm{e})}{\partial(\lambda,q)}\right|} \quad . \tag{51}$$

The exact description of the numerical details can be found in Speith et al. (1995). Nevertheless a short summary will be given in the following. At the beginning a certain gas ring with radius r_{e} is chosen, which makes it possible to calculate the mininimal and maximal redshift. For each single redshift on this ring, λ can be calculated by transforming Eq. 37. This is inserted in the integral equations (Eq. 26 - 28), where the only unknown quantity is q. Solving this numerically for each case, we filter the photons with a certain (g^*, r_{e}), which actually hit the observer. Now the motions are fully determined and we can derive the derivative of Eq. 51 numerically in order to calculate the *Transferfunction*. As we built the accretion disk out of many gas rings, we have to repeat this procedure for their different r_{e}.

3 Different Models

In the following section, the different models and their approximations are presented. They are all designed to fit spectra, which sets the upper limit of the duration of one line calculation to a few seconds. This is compared to exact simulations of the line shape, which usually last around three magnitudes longer. All models are normalized, such that the area below each the curves for a specific inclination angle is the same.

All models are calculated for a maximum rotating black hole ($a = 0.998$) and a fixed emissivity $\beta = \sqrt{r}$. Furthermore photons from the radius of marginal stability $r_{\mathrm{ms}} = 1.235\,GM\mathrm{c}^{-2}$ down to $r = 50\,GM\mathrm{c}^{-2}$ are used for integrating the line profile. Additionally the exact simulation uses a Gaussian emission line at $E_0 = 6.4\,\mathrm{keV}$ with a narrow width of $\sigma_0 = 0.01 E_0$ in the rest frame of the disk.

3.1 `laor`

The majority of publications use the `Laor` model, which was the first model for a spinning black hole and was calculated by Laor (1991) for a fixed $a = 0.998$. This clearly limits the possibilities and does not allow any determination of the black hole spin. Moreover only a small grid of transfer functions and no interpolation techniques are integrated in the model. Figure 6 shows a comparison for different viewing angles θ (measured with respect to the accretion disk) to the exact calculation.

Although the line shape seems crude, it fits the exact calculation well for higher inclination angles as the line shape is smooth. For lower angles, where the peaks become more narrow and stronger the `Laor` model lacks to describe the dynamic features. Despite strong differences between $\theta = 5^{\mathrm{o}}$ and $\theta = 10^{\mathrm{o}}$ in the exact model, there is hardly any difference in the model besides a slightly different normalization.

3.2 `kyrline`

Dovčiak et al. (2004) designed the `kyrline` model, which uses a huge table of transfer functions. This serves to calculate the line shape fast and without interpolation like Laor, but with a much higher resolution. Additionally a is variable for fitting the spin of a black hole. The comparison can be seen in Figure 7.

The model fits the exact calculation for all inclination angles and even at the narrow peaks. Although not really smooth, the line shape in a spectrum can be modeled with sufficient accuracy.
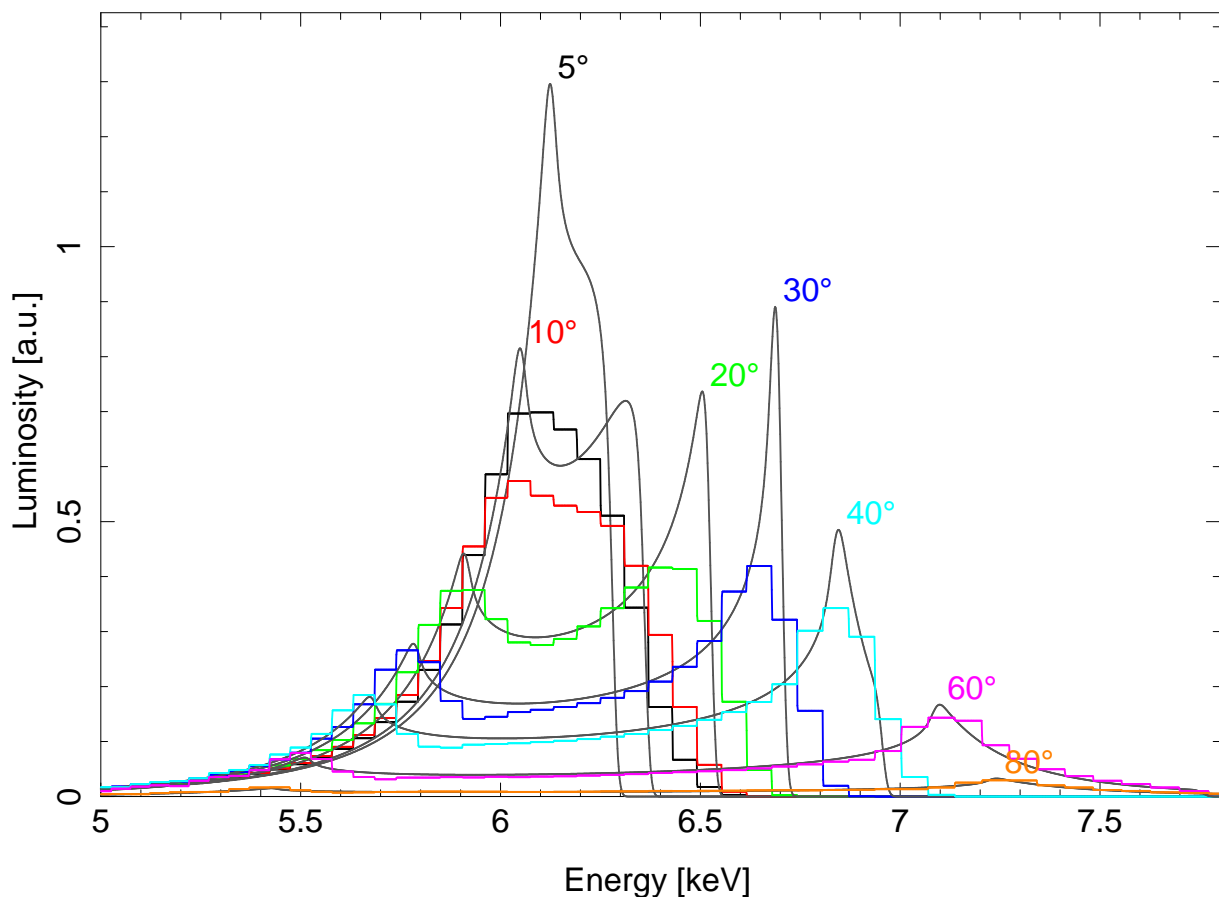
Figure 6: Comparison of the `laor` model (steps) to the exact calculation (grey) for different viewing angles θ measured with respect to the accretion disk.

3.3 `kerrdisk`

Stating that the model of Dovčiak et al. (2004) is too large and still not smooth, Brenneman & Reynolds (2006) invented a model which uses a comparably small sized table and interpolation techniques. The fact that the transfer function is very smooth, allows them to interpolate several points between two data points. The `kerrdisk` model is plotted in Figure 8.

The line profiles do not look as smooth as `kyrline`, but exhbit spikes, which can be seen best for lower incliniation angle. In contrast to the `laor` model the overall shape of the emission line fits better. Not only more values are calculated, but also the peaks are more pronounced.

similar to the `laor` model described in section 3.1: At high inclination angles `kerrdisk` fits the exact calculations pretty well whereas for low angles the shape deviates more.
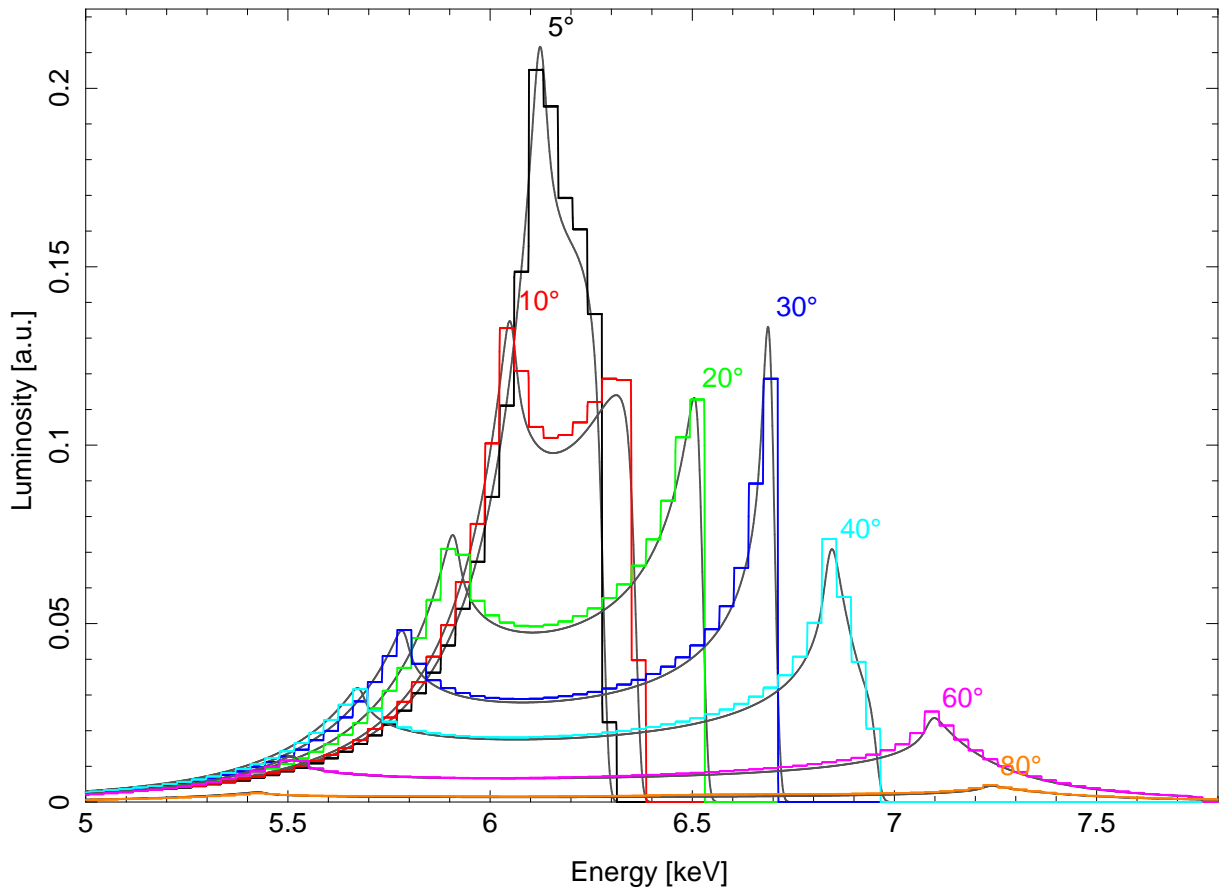
Figure 7: Comparison of the `kyrline` model (steps) to the exact calculation (grey) for different viewing angles θ measured with respect to the accretion disk.

4 Conclusion

4.1 Comparing the Different Models

The models in the section above were all calculated with the highest possible resolution of the single model. In order to compare them better, they are rebinned to the same grid with an energy resolution of $\simeq 3\,\%$. Moreover this describes the real situation better, which consists of a detector with fixed bins onto which the models are evaluated. Figure 9 shows this for a typical inclination angle of $\theta = 40°$ and emissivity of $\alpha = 3.0$. Looking at the figure, the differences ΔF clearly reveal, that the `laor` model predicts a different flux in almost every bin. Thus although the single deviations are not much, the whole line shape is calculated wrong. In contrast to that, the `kerrdisk` model describes the total line shape better, but gives a different flux almost randomly for a few bins. In the right plot for $a = 0.998$, these deviations could almost be interpreted as second peaks. By shifting the resolution, the wrong peaks shift in energy or disappear. Fitting with such a model might lead to higher χ^2 values. But the determined parameters should not deviate, as the overall shape fits. In contrast to that, the shape that the `laor` model predicts is not modeled correctly, which might lead to slightly different parameters. The `kyrline` model
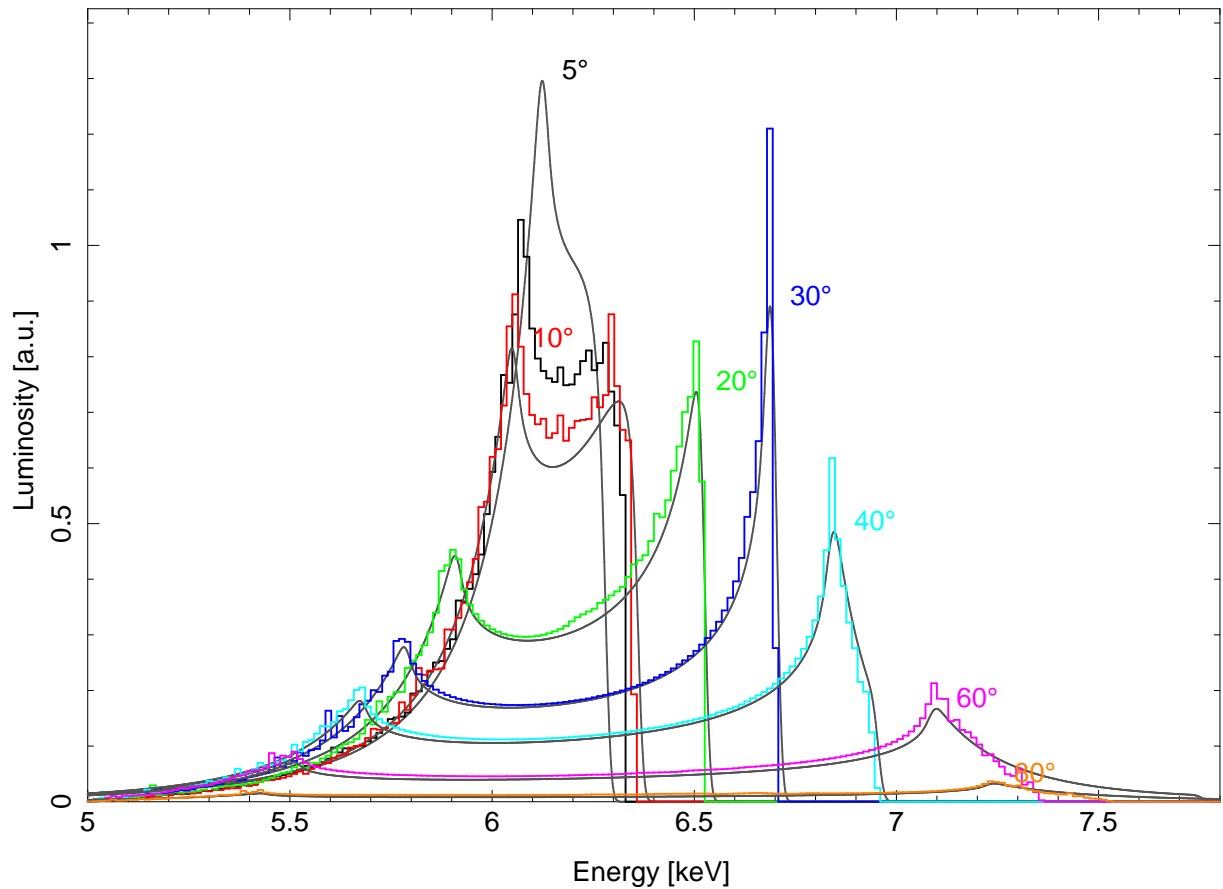
Figure 8: Comparison of the `kerrdisk` model to the exact calculation (grey) for different viewing angles θ measured with respect to the accretion disk.

follows the exact calculation almost perfect, except at some bins around the peak. This clearly leads to the conclusion that the `kyrline` model is best suited for fitting and that its huge sized precalculated tables are really necessary for providing the correct line shape.

4.2 Measuring the Spin

In order to state if it is possible to measure the spin of a black hole, an important indicator clearly is how much the shape of the line changes with respect to a. For this analysis, a typical inclination angle $\theta = 40°$ and a emissivity $\alpha = 3$ were chosen. As Figure 10 clearly shows, the blue peak does not change very much, but the red peak and the red tail get significantly brighter for increasing spin. Moreover this plot reveals that the line of a fast spinning black hole can be several keV in width, which makes it hard to distinguish the emission line from the continuum. Therefore the crucial issue for determining the spin correctly, is to understand the continuum spectrum as best as possible. Neglecting in Fig. 10 the spectrum below $3\,\mathrm{keV}$ and adding some noise, one can easily imagine that after renormalizing it can even become hard to distinguish between a maximally and non rotating black hole. Therefore it is really important to model the shape of the relativistic iron line with a high presission in order to draw conclusions about the
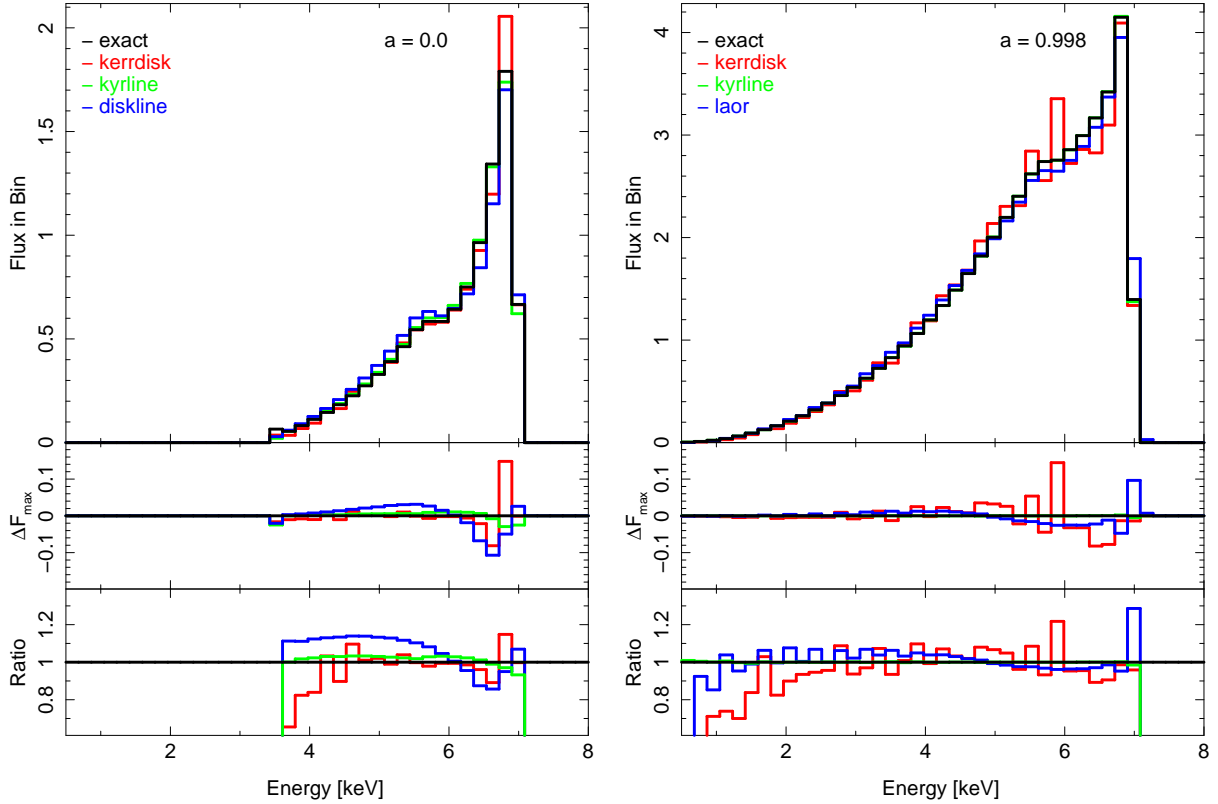
Figure 9: Comparison of the different line models on a grid with $\Delta E/E \approx 0.03$. A typical inclination angle of $\theta = 40°$ and emissivity of $\alpha = 3.0$ was chosen for this calculation.

spin of the black hole.

References

Bardeen J.M., Press W.H., Teukolsky S.A., 1972, ApJ 178, 347

Brenneman L.W., Reynolds C.S., 2006, ApJ 652, 1028

Carroll S.M., 2004, Spacetime and geometry. An introduction to general relativity

Carter B., 1968, Phys. Rev. 174, 1559

Chandrasekhar S., 1983, The mathematical theory of black holes

Cunningham C.T., 1975, ApJ 202, 788

Cunningham J.M., Bardeen C.T., 1973, ApJ 183, 237

Dovčiak M., Karas V., Yaqoob T., 2004, Astrophysical Journal Supplement 153, 205

Kerr R.P., 1963, Phys. Rev. Lett. 11, 237
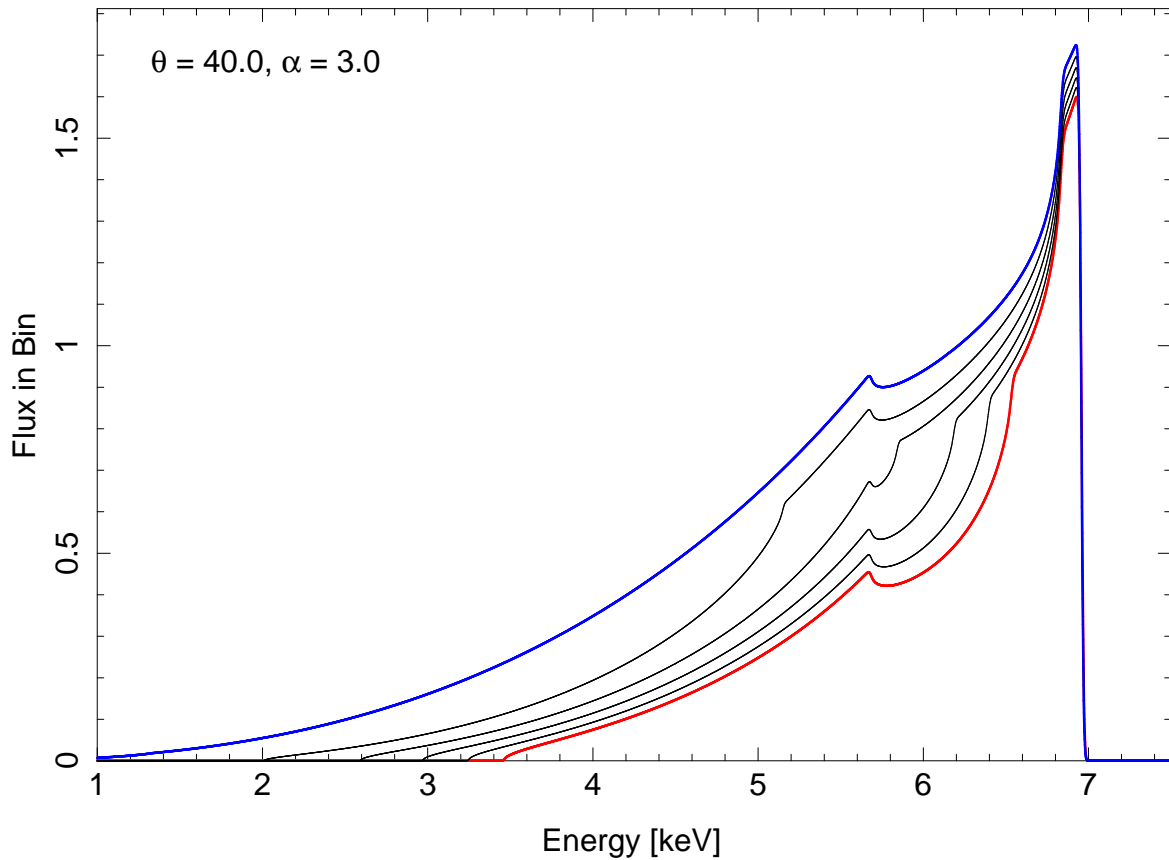
Figure 10: The dependency of the line shape on the spin of a black hole. Typical values of $\theta = 40°$ and $\alpha = 3$ were chosen.

Krolik J.H., 1999, Active galactic nuclei : from the central black hole to the galactic environment

Laor A., 1991, ApJ 376, 90

Miller J.M., 2007, Annual Review of Astronomy & Astrophysics 45, 441

Miniutti G., Fabian A.C., Anabuki N., et al., 2007, Publications of the Astronomical Society of Japan 59, 315

Misner C.W., Thorne K.S., Wheeler J.A., 1973, Gravitation

Reeves J.N., Fabian A.C., Kataoka J., et al., 2006, Astronomische Nachrichten 327, 1079

Reynolds C.S., 1996, Ph.D. Thesis, University of Cambridge

Speith R., Riffert H., Ruder H., 1995, Computer Physics Communications 88, 109

Svoboda J., Dovčiak M., Goosmann R., Karas V., 2009 507, 1

Thorne K.S., 1974, ApJ 191, 507